

The BTB domains of the potassium channel tetramerization domain proteins prevalently assume pentameric states

Giovanni Smaldone¹, Luciano Pirone^{2,3}, Emilia Pedone², Thomas Marlovits^{4,5,6,7}, Luigi Vitagliano² and Luciano Ciccarelli^{4,5,6,7}

1 IRCCS SDN, Napoli, Italy

2 Institute of Biostructures and Bioimaging, C.N.R., Napoli, Italy

3 Consorzio Interuniversitario di Ricerca in Chimica dei Metalli nei Sistemi Biologici (C.I.R.C.M.S.B.), Catania, Italy

4 Center for Structural Systems Biology (CSSB), University Medical Center Hamburg-Eppendorf (UKE), Hamburg, Germany

5 Deutsches Elektronen-Synchrotron (DESY), Hamburg, Germany

6 Institute of Molecular Biotechnology (IMBA), Austrian Academy of Sciences, Vienna, Austria

7 Research Institute of Molecular Pathology (IMP), Vienna, Austria

Correspondence

L. Vitagliano, Institute of Biostructures and Bioimaging, C.N.R., IBB-CNR Via Mezzocannone 16, Napoli 80134, Italy
Tel/Fax: +39 0812534506
E-mail: luigi.vitagliano@unina.it
and

L. Ciccarelli, Institute of Molecular Biotechnology (IMBA), Dr. Bohr-Gasse 3-7, Room 6.14 1030 Vienna, Austria
Fax: +43 1 790 44 110
Tel: +43 1 790 44 4641
E-mail: luciano.ciccarelli@imba.oeaw.ac.at

(Received 8 February 2016, revised 21 April 2016, accepted 26 April 2016, available online 24 May 2016)

doi:10.1002/1873-3468.12203

Edited by Miguel De la Rosa

Potassium channel tetramerization domain-containing (KCTD) proteins are involved in fundamental physio-pathological processes. Here, we report an analysis of the oligomeric state of the Bric-à-brack, Tram-track, Broad complex (BTB) domains of seven distinct KCTDs belonging to five major clades of the family evolution tree. Despite their functional and sequence variability, present electron microscopy data highlight the occurrence of well-defined pentameric states for all domains. Our data also show that these states coexist with alternative forms which include open pentamers. Thermal denaturation analyses conducted using KCTD1 as a model suggest that, in these proteins, different domains cooperate to their overall stability. Finally, negative-stain electron micrographs of KCTD6^{BTB} in complex with Cullin3 show the presence of assemblies with a five-pointed pinwheel shape.

Keywords: electron microscopy; protein oligomerization; protein structure; thermal stability

Oligomerization is a widespread phenomenon among proteins of all kingdoms of life. The tendency of proteins to assemble in multimeric states increases with the complexity of the living organism [1]. The wide occurrence of protein multimerization has been related to the many advantages that it offers. These include higher stabilities against proteases and the possibility of finer regulations. Although multimerization can be mediated by a huge number of protein folds, in some

modular proteins this process is delegated to domains specialized in this task. Intriguingly, the same oligomerization domain is frequently able to promote multimerization in proteins involved in different biological functions and characterized by unrelated structural organizations. In this scenario, the Bric-à-brack, Tram-track, Broad complex (BTB) domain is one of the best characterized oligomerization domains [2]. Although structural variations among BTB domains are

Abbreviations

BTB, Bric-à-brack, Tram-track, Broad complex; CD, circular dichroism; Cul3, cullin 3; EM, electron microscopy; KCTD, potassium channel tetramerization domain proteins; SEC, size exclusion chromatography; SP, single particle.

observed, they share a conserved structural motif constituted by five helices and a three-stranded β -sheet. BTB domains have been detected in a variety of protein families which include BTB-zinc finger, BTB-BACK-kelch, voltage-gated potassium channel T1, and potassium channel tetramerization domain-containing (KCTD) proteins [2]. BTB domains mediate both hetero- and homo-oligomerization. BTB-mediated homo-oligomerization may lead to the formation of a variety of structural assemblies which include monomeric, dimeric, tetrameric, and pentameric states.

Among BTB-containing proteins, the KCTD family represents an emerging class of proteins involved in fundamental physio-pathological processes [3,4]. Indeed, KCTD members are involved in a variety of diverse biological function processes which include, among others, protein ubiquitination and degradation [5–8], suppression of proliferation or transcription [9–11], human genetic disease risk [12,13], sleep homeostasis [14], and regulation of G-protein-coupled receptors [15–18].

Despite their biological roles, a full understanding of the mechanisms underlying the functions of KCTD proteins is hampered by the limited molecular/structural data available. The 25 members of the family share a common BTB domain which is frequently coupled with a highly variable C-terminal domain. The analysis of BTB similarities of KCTDs indicates that they exhibit sequence identities in the range 30–80%. Although most of the biophysical/structural characterizations of KCTDs hitherto reported have been focused on the BTB domains, some of their basic properties remain to be elucidated as even their oligomerization state is somewhat uncertain. Although low-resolution solution studies and molecular modeling indicated that some BTB domains of the KCTD family could assemble in tetramers as the closely related T1 domains of the T1 voltage-gated potassium channels, available crystallographic data suggest other possibilities. Indeed, the first crystal structure of a KCTD protein shows that both the BTB and the entire protein form well-defined pentamers [19]. Moreover, in the crystal structures of the BTB domains of KCTD proteins, SHKBP1, KCTD10, KCTD13, KCTD16, and KCTD17, recently deposited in the Protein Data Bank (codes 4CRH, 5FTA, 4UIJ, 5A15, and 5A6R) but not described in any publication, the oligomeric state has been assigned as monomeric. However, the visual inspections of some of these structures suggest the formation of larger aggregates. Indeed, while SHKBP1 does not form any oligomer, KCTD10^{BTB} (distorted tetramer), KCTD13^{BTB} (distorted tetramer), KCTD16^{BTB} (open pentamers), and KCTD17^{BTB} (closed pentamers) seem

to form higher oligomers. Finally, the crystal structures of the BTB domains of KCTD1 and KCTD9, which were published while this manuscript was in preparation, also present a pentameric association [20]. This important contribution also unraveled that KCTD1^{BTB} forms peculiar open pentameric states. This study also suggests the occurrences of pentameric states for the BTB domains of KCTD6 and KCTD17. However, according to the authors, this observation needs to be validated by further experimental studies [20]. In this puzzling scenario, we report here an analysis of the oligomeric state of the BTB domains of seven distinct KCTD proteins belonging to five major clades of the family evolution tree (see the related figures in refs. [3,4,20]). In particular, we studied the BTB domain of members of Clade A (KCTD1 and KCTD15), Clade B (KCTD6 and KCTD11), Clade C (KCTD13), Clade E (KCTD5), and Clade F (KCTD12). This ensemble includes both cullin 3 (Cul3)-binding (KCTD5, KCTD6, KCTD11, and KCTD13) and Cul3-independent (KCTD1, KCTD12, and KCTD15) proteins [21]. These proteins are involved in unrelated biological processes which include GABA(B) receptor regulation (KCTD12) [15,16], neural crest domain regulation (KCTD1 and KCTD15) [11], and ubiquitination/degradation (KCTD5, KCTD6, KCTD11, and KCTD13) of a variety of different substrates such as HDAC1, RHOA, and sAnk1.5 [6–8,22].

Despite the functional/sequence variability of these domains (Table 1), the present electron microscopy (EM) analyses highlight the presence of well-defined pentameric states for all of them. In line with the results recently reported by Privé and coworkers [20], we also detected some level of structural heterogeneity in the investigated samples. Using KCTD1 as a model we show that the C-terminal domain can stabilize the structure of the BTB domain in these proteins. These observations suggest that the heterogeneity observed may, at least in part, be due to the dissection of the protein in individual domains. This study complements and expands the recent results obtained by Ji *et al.* [20] and clearly indicates that the pentameric state likely represents the prevalent functional oligomeric state of the BTB domain of KCTD proteins in their functional states.

Materials and methods

Protein expression and purification

The BTB domains of KCTD5 (residues 44–145, KCTD5^{BTB}), KCTD6 (residues 10–110, KCTD6^{BTB}), KCTD11 (residues 15–116, KCTD11^{BTB}), KCTD12

Table 1. Percentages of sequence identity of the BTB domains of the KCTD members characterized in this study. The number of aligned residues for each pair has been reported in the brackets. The BTB domains whose structure has been determined by X-ray crystallography are underlined.

BTB domain	<u>KCTD1</u>	<u>KCTD5</u>	KCTD6	KCTD11	KCTD12	<u>KCTD13</u>	KCTD15
KCTD1		32% (91)	54% (91)	44% (94)	39% (91)	30% (90)	81% (97)
KCTD5			41% (96)	40% (100)	34% (92)	36% (94)	34% (91)
KCTD6				61% (99)	44% (100)	43% (90)	57% (90)
KCTD11					40% (103)	43% (94)	43% (100)
KCTD12						36% (91)	42% (97)
KCTD13							30% (97)
KCTD15							

(residues 27–131, KCTD12^{BTB}), and KCTD15 (residues 61–157, KCTD15^{BTB}) were expressed in *Escherichia coli* BL21(DE3) and were purified by following the previously reported protocols [5,21,23–26]. Similarly, Cul3^{NTD}, which corresponds to the N-terminal region (residues 20–381) of Cul3, was expressed and purified according to the procedure reported by Balasco *et al.* [23].

The procedures adopted for the newly expressed full-length KCTD1 proteins (UniProt code [Q719H9](#) residues 1–257), and its BTB domain (residues 1–135, KCTD1^{BTB}), and the BTB domain of KCTD13 (UniProt Code [Q8WZ19](#), residues 1–135, KCTD13^{BTB}) are reported in the supplementary material.

Solution studies

KCTD1^{BTB}, KCTD5^{BTB}, KCTD6^{BTB}, KCTD11^{BTB}, KCTD12^{BTB}, KCTD13^{BTB}, and KCTD15^{BTB}, initially stored in a buffer containing 50 mM TrisHCl and 200 mM NaCl (pH 7.5), were loaded on a Superdex 200 10/30 (GE Healthcare, Bioscience AB, Uppsala, Sweden) column previously equilibrated with the buffer used for storage. In the case of KCTD12^{BTB}, which has a tendency to form covalent aggregates, the reducing agent DTT at 2 mM concentration was also added to the experimental media.

The estimations of the molecular weights was performed upon column calibration with the Gel Filtration calibration kit (GE Healthcare). The markers contained in this kit are blue dextran 2000 (Mw > 1000 kDa, elution volume 7.8 mL), ovalbumin (Mw 43 kDa, elution volume 14.9 mL), carbonic anhydrase (Mw 29 kDa, elution volume 15.6 mL), and ribonuclease A (Mw 13.7 kDa, elution volume 17.2 mL).

The correct folding of all proteins was assessed by Far-UV circular dichroism (CD) spectroscopy. The spectra were recorded in the 190–260-nm range on a Jasco J-710 spectropolarimeter equipped with a Peltier thermostatic cell holder [Jasco Europe, Cremella (LC), Italy model PTC-343]. The spectra were registered under a constant N₂ flow carried out at 20° using the following experimental

parameters: scanning speed of 20 nm·min⁻¹, band width of 2 nm, and response time of 4 s. In all cases the protein concentration was 0.3 mg·mL⁻¹.

Thermal denaturation curves of KCTD1 (and KCTD1^{BTB}) and KCTD13^{BTB} were recorded over the 20 °C–100 °C temperature interval monitoring the CD signal at 222 nm. The curve was registered using a 0.1-cm path length cell, a protein concentration of 3 μM, and a scan rate of 1.0 °C·min⁻¹.

Negative staining

Electron microscopy samples were prepared by applying a protein solution (3 μL) on previously glow-discharged carbon-coated copper grids and negatively stained with uranyl acetate 2%. Dilutions were optimized to ensure a good distribution of the particles across the grid; the final concentration of protein sample used was typically 0.05 mg·mL⁻¹.

Electron microscopy

Grids were imaged under low-dose conditions with a Tecnai Morgani 80 KV electron microscope at a defocus range of 2.0–5.0 μm and at a nominal magnification of 30 000× resulting in a pixel size of 3.0 Å on the specimen. Particles were extracted by e2boxer [27] either in semi-automated (KCTD5^{BTB}, KCTD6^{BTB}, KCTD12^{BTB}, KCTD13^{BTB}, and KCTD15^{BTB}) or manual mode (KCTD1^{BTB}, and KCTD11^{BTB}); in the latter case only top views were selected to facilitate the image processing aimed at the characterization of the oligomeric state, which is possible only with particles in top views. The number of particles boxed out from micrographs for each protein, either manually or semiautomatically, is reported in Table 2. As a common image-processing strategy, single-particle (SP) images of each sample were subjected to a first round of 2D reference-free class averaging with EMAN2 in order to exclude from the dataset ‘bad’ particles forming not significant classes. Then, a second round of 2D reference-free class averaging was performed and the resulting classes were used for data analysis. Rotational cross-correlation analysis

was performed with IMAGIC-5 (Image Science Software GmbH, Berlin, Germany).

Results

Solution studies

Preliminary insights on the dimensions of the BTB domains isolated from KCTD1, KCTD5, KCTD6, KCTD11, KCTD12, KCTD13, and KCTD15 were obtained by performing analytical SEC analyses using a Superdex 200 10/30 column. As shown in Fig. 1, for most of the proteins the elution volume falls in the interval 13.7–15.0 mL. The corresponding MW_{app} range is 48–75 kDa. The formal number of chains is between 3.1 (for KCTD15^{BTB}) and 5.2 (for KCTD11^{BTB}). The number of chains for KCTD1^{BTB} (3.7), KCTD5^{BTB} (4.3), KCTD6^{BTB} (4.2), and KCTD12^{BTB} (4.7) assumes intermediate values. A significantly different behavior is displayed by KCTD13^{BTB} (Fig. 1) which presents a much higher elution volume (17.5 mL). This result indicates that the oligomeric assembly of this domain is likely unstable.

The folding state of all domains was determined by Far-UV CD spectroscopy. The spectra of KCTD5^{BTB}, KCTD6^{BTB}, KCTD11^{BTB}, KCTD12^{BTB}, and KCTD15^{BTB} are very similar to those we reported in previous characterizations and are indicative of well-folded α/β domains. The CD spectra of the newly expressed domains, KCTD1^{BTB} and KCTD13^{BTB} (Fig. 2A), show that they also assume the expected α/β fold. The minimum and the shoulder exhibited by the KCTD13^{BTB} domain are at slightly shorter wavelength when compared to those shown by KCTD1^{BTB} (Fig. 2A). This may be indicative of a less stable state for this domain. To assess this possibility we performed thermal denaturation analyses of both KCTD13^{BTB} (Fig. 2B) and KCTD1^{BTB} (Fig. 2C). The evolution of the CD signal upon heating indicates that KCTD13^{BTB} rapidly unfolds. This observation indicates that this domain is endowed with a very limited stability at room temperature and also explains the anomalous behavior detected in the SEC analysis.

In contrast, KCTD1^{BTB} is rather stable with a melting temperature of 57 °C. Since we were able to express full-length KCTD1 in high yields, we also

Table 2. Number of micrographs and number of the extracted particles for the BTB samples.

	KCTD1 ^{BTB}	KCTD5 ^{BTB}	KCTD6 ^{BTB}	KCTD11 ^{BTB}	KCTD12 ^{BTB}	KCTD13 ^{BTB}	KCTD15 ^{BTB}
Number of micrographs	21	21	16	15	9	17	24
Particles dataset	253	3500	1366	382	2800	132	674

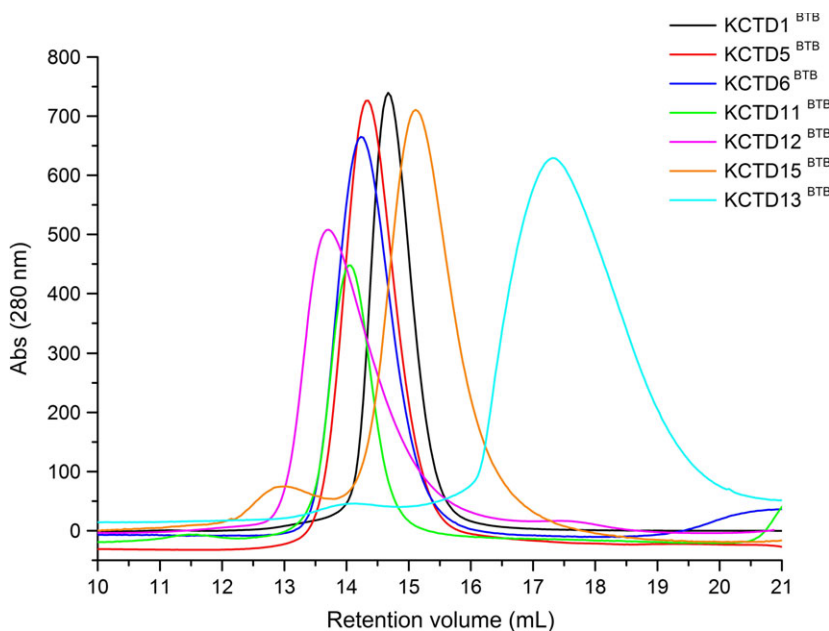


Fig. 1. Analytical size exclusion chromatography of the BTB domain of various members of the KCTD family.

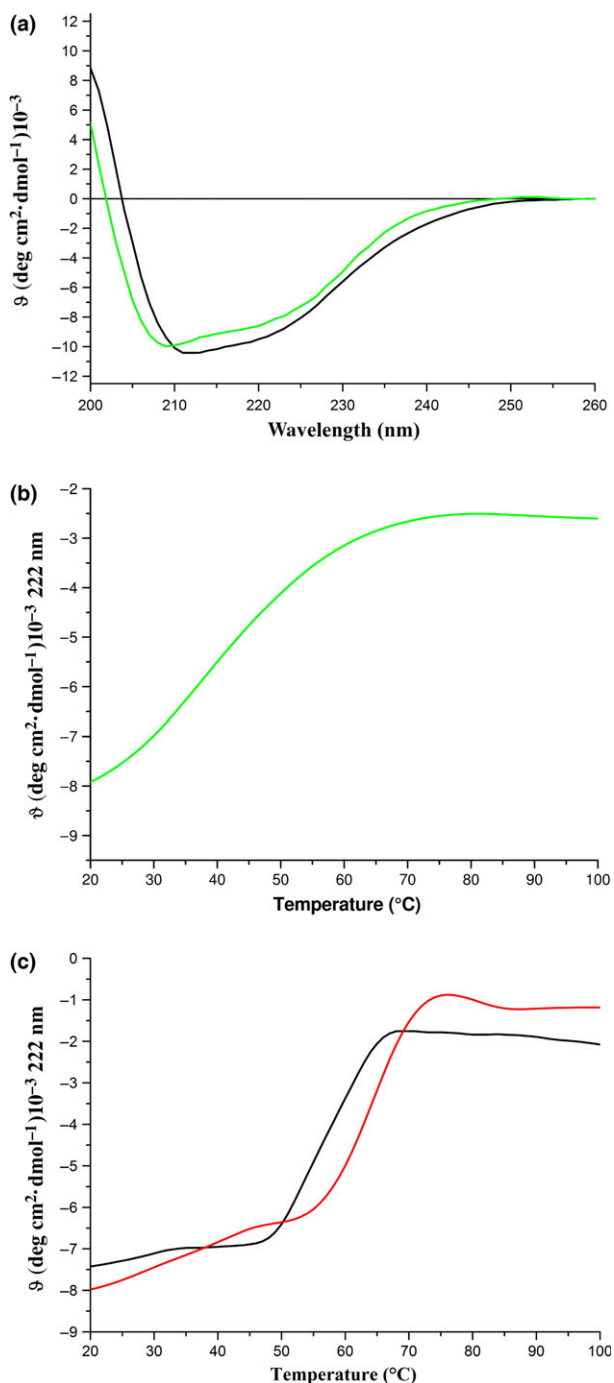


Fig. 2. Circular dichroism analysis. Far-UV spectra of KCTD1^{BTB} (black) and KCTD13^{BTB} (green) (A). Thermal denaturation curves of KCTD13^{BTB} (B) and of KCTD1^{BTB} (black line)/KCTD1 full-length (red line) (C).

analyzed the CD properties of this protein. The Far-UV spectrum of KCTD1 (Fig. S1) is similar to the one corresponding to KCTD1^{BTB}. This suggests that also the C-terminal region of the protein assumes an α/β

fold. This observation is corroborated by a secondary structure prediction analysis carried out using the PSIPRED server (<http://bioinf.cs.ucl.ac.uk/psipred/>) that confirms the presence of both helices and strands in the protein C-terminus (Fig. S2). Interestingly, the thermal denaturation curve of full-length KCTD1 evidences the presence of a single major transition centered at 64 °C (Fig. 2C). This finding indicates that the presence of the C-terminal region increases the thermal stability of KCTD1^{BTB}. It is worth mentioning, however, that all thermal denaturations reported in Fig. 2B,C were not reversible.

Negative staining analysis

With negative stain, EM, protein samples are embedded in a thin and dried layer of heavy metal salt that increases the contrast [28]. This allows relatively small protein samples to be visualized for different purposes. In order to see whether SP analysis of negative stained KCTDs could be used to gain insights into the oligomeric state of relatively small oligomeric proteins such as the BTB domains of KCTDs, we used negative stain method (Figs 3A and S3A) and subsequently performed 2D reference-free class averaging on KCTD5^{BTB} (Figs 3B and S3B), whose pentameric state is well established in both its isolated state and in the context of the entire KCTD5 protein [19].

Notably, pentameric-shaped particles for KCTD5^{BTB} could be easily recognized even in the raw electron micrographs (Figs 3A and S3A). This observation is corroborated by the analysis of the class averages with increased signal-to-noise ratio which shows the prevalence of pentamers for particles lying in top view on the grid carbon support (Fig. S3B). The pentameric state of some of these classes is clearly confirmed by the rotational cross-correlation analysis (Fig. S3C). It is worth mentioning that, along with closed pentamers, the analysis of the class averages also highlights the occurrence of open pentameric and putative tetrameric states (Fig. S3B). Encouraged by the result of SP analysis on KCTD5^{BTB}, we applied this approach also to KCTD1^{BTB} whose pentameric state has been recently detected by X-ray crystallography [20]. As shown in Figs 3B and S4, the 2D reference-free class averages indicate that also KCTD1^{BTB} forms pentamers thus corroborating the literature crystallographic data. Interestingly, the extension of this approach to proteins for which previous analyses suggested a tetrameric state (KCTD6^{BTB}, KCTD11^{BTB}, KCTD12^{BTB}, and KCTD15^{BTB}) also revealed the presence of the pentameric states (Figs 3B and S5–S9).

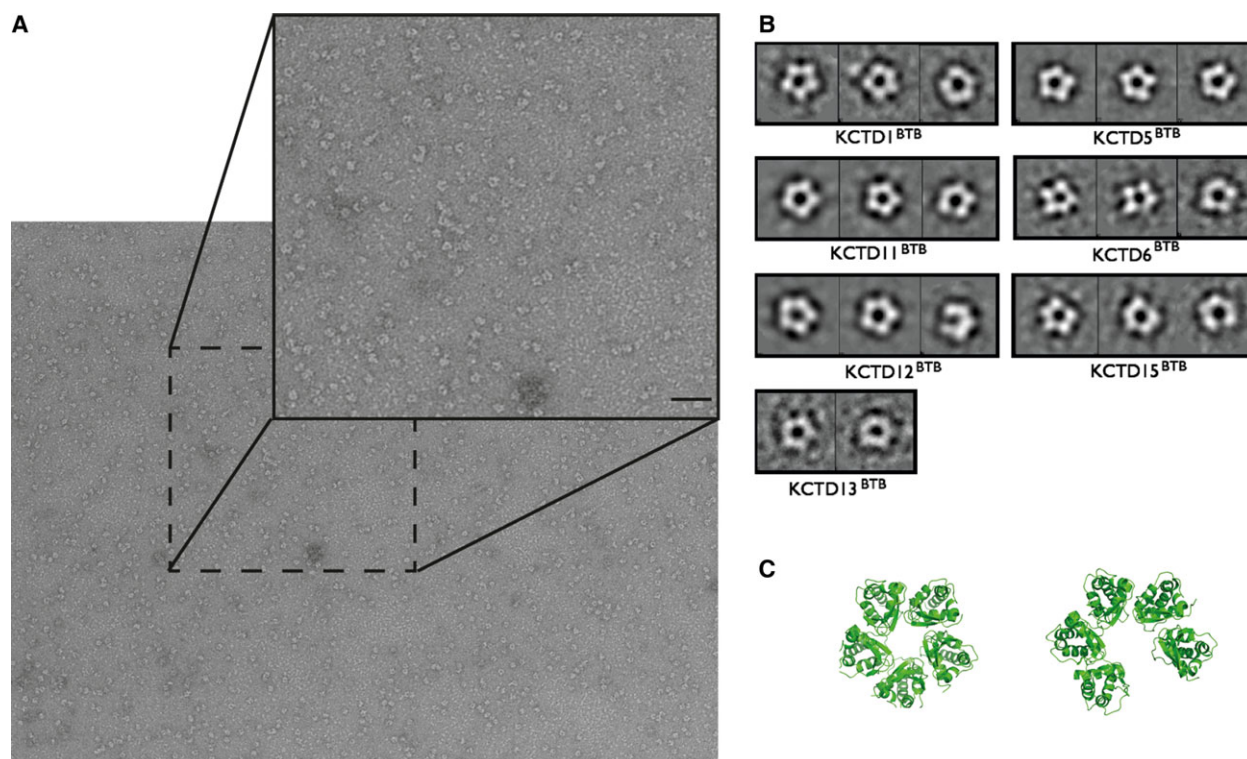


Fig. 3. Electron micrograph of the KCTD5^{BTB} domain and 2D reference-free class averages of KCTD^{BTB} domains. In panel (A), a negative-stain electron micrograph of KCTD5^{BTB} sample. In panel (B), 2D reference-free class averages of particles lying on the carbon support of the microscopy grid in top views revealed a pentameric state for KCTD1^{BTB}, KCTD5^{BTB}, KCTD6^{BTB}, KCTD11^{BTB}, KCTD12^{BTB}, KCTD13^{BTB}, and KCTD15^{BTB}. In panel (C), the crystal structure of KCTD1^{BTB} closed and open pentamers are shown in top views for comparative purposes. Scale bar: 20 nm.

The analysis of KCTD13^{BTB} shows the presence of pentamers along with a larger structural heterogeneity (Figs 3B and S8). Indeed, for this protein a very limited number of particles could be considered in the class averages (Table 2). Consequently, only three class averages could be derived for KCTD13^{BTB} (Fig. S8C). This observation suggests that other (smaller) species might be present in the sample. This finding is in line with the results of the SEC analysis and with the CD data which indicate that this domain is barely stable at room temperature (see above).

Altogether these findings strongly suggest that pentamers are common among the BTB domains of the KCTD proteins. In this context, it is important to point out that as no symmetry was applied, the result comes only from the dataset itself without any *a priori* assumption of symmetry based on previous data or sequence similarity. An advantage of this approach is that conformational variability and sample heterogeneity can be detected. Indeed, class averages of the different KCTD^{BTB} particles revealed a certain degree of flexibility that perturbs the ‘perfect’ pentameric

symmetry of the protein complexes. Indeed, as for KCTD5^{BTB}, in KCTD6^{BTB}, KCTD12^{BTB}, and KCTD15^{BTB} pentameric states coexists with open pentameric states (Figs S3C, S5C, S7C, and S9C) which reminds the open state of KCTD1 reported by Privé and coworkers [20]. For KCTD6^{BTB}, KCTD12^{BTB}, and KCTD15^{BTB} smaller (putative) tetrameric states were also observed.

Once the oligomeric states of KCTD^{BTB} domains were characterized, we used negative staining EM to study the complexes that KCTD proteins form with their biological partners. In particular, we analyzed the complex that KCTD6^{BTB} forms with the N-terminal region (residues 20–381) of Cul3 (Cul3^{NTD}). Notably, raw negative-stain electron micrographs of KCTD6^{BTB} in complex with Cul3^{NTD} clearly show the presence of aggregates with a five-pointed pinwheel shape (Fig. 4) we previously suggested for the complex between KCTD5 and Cul3 [23] and recently observed in the cryo EM study of the complex between KCTD9 and Cul3 [20]. The size of these aggregates (~ 200 Å) is in line with that expected on the basis of the molecular

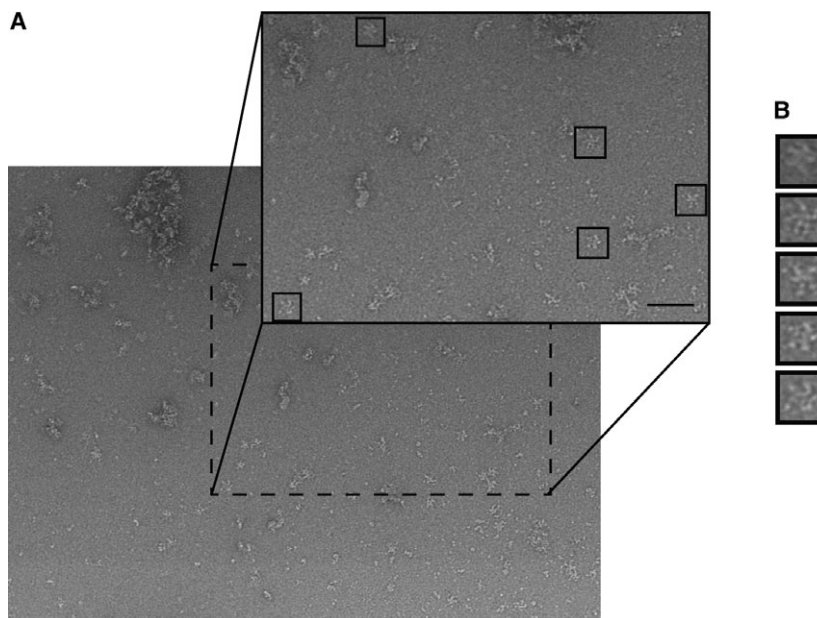


Fig. 4. Negative-stain electron micrograph of the complex KCTD6^{BTB}-Cul3^{NTD}. The pentameric state of KCTD6^{BTB} is evident in raw electron micrograph of the 5 : 5 complex with Cul3^{NTD}. Heterodecamers are reported in top view of the boxes (A). In panel (B) some individual particles are shown. Scale bar: 20 nm.

modeling [23]. These results confirm the pentameric nature of KCTD6^{BTB} and, simultaneously, the 5 : 5 stoichiometry of the KCTD6^{BTB} – Cul3^{NTD} complex. A deep inspection of the micrographs (Fig. 4) unravels that distinct Cul3^{NTD} molecules assume different orientations. This indicates that Cul3 is endowed with a remarkable flexibility in these complexes.

Discussion

The BTB domain represents the unifying structural motif among the members of the KCTD family. In these proteins, not only does the BTB domain promote oligomerization but it also constitutes the binding unit for important biological partners. Indeed, BTB multimerization creates the recognition surface for interactors such as Cul3 [21], Ap-2 [11], and GABA(B) receptors [15,16]. We addressed here the debated issue related to the BTB oligomerization state. The present extensive EM analysis clearly indicates that, despite the homology with the T1 KCTD, a number of BTB domains of functionally unrelated KCTD proteins assumes pentameric states. Taking also into account the crystallographic pentameric structures of KCTD1^{BTB} [20], KCTD5^{BTB} [19], KCTD9^{BTB} [20], and KCTD17^{BTB} (PDB code 5ACR) and the close identity of KCTD members of the same evolutionary clade, present finding suggests that the pentameric organization is a rather general property among these proteins. Notably, present data also indicate that, in addition to well-defined closed pentameric states, these domains exhibit a significant level of structural

heterogeneity. In line with the crystallographic data on KCTD1^{BTB} [20] and KCTD16^{BTB} (PDB code 5A15) which are able to form open pentamers, we frequently observe open pentameric rings in the micrographs as well as in the class averages of our proteins. Moreover, we occasionally detected smaller tetrameric-like states. This finding is not surprising as distorted tetrameric states have been recently reported for KCTD10^{BTB} and KCTD13^{BTB} (PDB codes 5FTA and 4UIJ). In this intricate scenario, it is worth mentioning that SHKBP1, a member of the Clade D, assumes a monomeric structure in the crystal state (PDB code 4CRH).

These observations open an important question related to the source of this heterogeneity. In particular, is it a peculiar, even functional, property of these domains or is it an artifact due to KCTD dissection in individual domains? Using KCTD1 as model system we here show that the stability of the BTB domain is increased by the concomitant presence of the protein C-terminal domain. Although further studies are required to fully address this issue, this finding suggests that, in these proteins, the different domains may cooperate to assure structural stability. An analogous consideration has been used to explain the higher affinity of full-length KCTD5 for Cul3 compared to KCTD5^{BTB} [20]. The possibility to form open structures is nevertheless an interesting property of these domains. Indeed, it suggests that these proteins retain folded chains even when the quaternary structure is perturbed. This may endow these domains with a structural versatility that can be exploited for establishing functional interactions.

From the methodological point of view, our analysis indicates that rather simple approaches such as the negative staining raw images and SP 2D class averaging analysis may provide valuable information into the oligomeric state of relatively small proteins. It is worth mentioning that the assessment of protein oligomeric state is often a cumbersome issue. It should be noted that a full characterization of the different structural states such as those observed from the recently obtained crystal structure of KCTD1 [20] cannot be properly investigated with negative-stain SP analysis due to resolution limits. However, our results are encouraging for KCTD high-resolution studies by cryo-electron microscopy, which, thanks to technological advances can be currently performed also on relatively small proteins (< 200 kDa). The application of this technique may indeed provide quantitative details on aspects such as the Cul3 flexibility emerged from this study (Fig. 4). Indeed, as already suggested for the KCTD counterpart [29], the flexibility of the cullin may play an important role in the functionality of these large macromolecular assemblies.

Acknowledgements

The financial support of Regione Campania (Bando POR per la Realizzazione della Rete delle Biotecnologie in Campania – progetto FARMABIONET) is acknowledged. The authors declare that no conflict of interest occurs.

Author contributions

GS, LP, and LC performed experiments, GS, LP, EP, TM, LV, and LC analyzed data, LV and LC conceived the experiments and wrote the manuscript.

References

- 1 Apic G, Gough J and Teichmann SA (2001) Domain combinations in archaeal, eubacterial and eukaryotic proteomes. *J Mol Biol* **310**, 311–325.
- 2 Stogios PJ, Downs GS, Jauhal JJ, Nandra SK and Prive GG (2005) Sequence and structural analysis of BTB domain proteins. *Genome Biol* **6**, R82.
- 3 Liu Z, Xiang Y and Sun G (2013) The KCTD family of proteins: structure, function, disease relevance. *Cell Biosci* **3**, 45.
- 4 Skoblov M, Marakhonov A, Marakasova E, Guskova A, Chandhoke V, Birerdinc A and Baranova A (2013) Protein partners of KCTD proteins provide insights about their functional roles in cell differentiation and vertebrate development. *Bioessays* **35**, 586–596.
- 5 Correale S, Pirone L, Di Marcotullio L, De Smaele E, Greco A, Mazzà D, Moretti M, Alterio V, Vitagliano L, Di Gaetano S *et al.* (2011) Molecular organization of the cullin E3 ligase adaptor KCTD11. *Biochimie* **93**, 715–724.
- 6 Canettieri G, Di Marcotullio L, Greco A, Coni S, Antonucci L, Infante P, Pietrosanti L, De Smaele E, Ferretti E, Miele E *et al.* (2010) Histone deacetylase and Cullin3-REN(KCTD11) ubiquitin ligase interplay regulates Hedgehog signalling through Gli acetylation. *Nat Cell Biol* **12**, 132–142.
- 7 De Smaele E, Di Marcotullio L, Moretti M, Pelloni M, Occhione MA, Infante P, Cucchi D, Greco A, Pietrosanti L, Todorovic J *et al.* (2011) Identification and characterization of KCASH2 and KCASH3, 2 novel Cullin3 adaptors suppressing histone deacetylase and Hedgehog activity in medulloblastoma. *Neoplasia* **13**, 374–385.
- 8 Chen Y, Yang Z, Meng M, Zhao Y, Dong N, Yan H, Liu L, Ding M, Peng HB and Shao F (2009) Cullin mediates degradation of RhoA through evolutionarily conserved BTB adaptors to control actin cytoskeleton structure and cell movement. *Mol Cell* **35**, 841–855.
- 9 Birerdinc A, Nohelty E, Marakhonov A, Manyam G, Panov I, Coon S, Nikitin E, Skoblov M, Chandhoke V and Baranova A (2010) Pro-apoptotic and antiproliferative activity of human KCNKG, a putative tumor suppressor in 13q14 region. *Tumour Biol* **31**, 33–45.
- 10 Ding X, Luo C, Zhou J, Zhong Y, Hu X, Zhou F, Ren K, Gan L, He A, Zhu J *et al.* (2009) The interaction of KCTD1 with transcription factor AP-2alpha inhibits its transactivation. *J Cell Biochem* **106**, 285–295.
- 11 Zarelli VE and Dawid IB (2013) Inhibition of neural crest formation by Kctd15 involves regulation of transcription factor AP-2. *Proc Natl Acad Sci USA* **110**, 2870–2875.
- 12 Golzio C, Willer J, Talkowski ME, Oh EC, Taniguchi Y, Jacquemont S, Raymond A, Sun M, Sawa A, Gusella JF *et al.* (2012) KCTD13 is a major driver of mirrored neuroanatomical phenotypes of the 16p11.2 copy number variant. *Nature* **485**, 363–367.
- 13 Marneros AG, Beck AE, Turner EH, McMillin MJ, Edwards MJ, Field M, de Macena Sobreira NL, Perez AB, Fortes JA, Lampe AK *et al.* (2013) Mutations in KCTD1 cause scalp-ear-nipple syndrome. *Am J Hum Genet* **92**, 621–626.
- 14 Pfeiffenberger C and Allada R (2012) Cul3 and the BTB adaptor insomnia are key regulators of sleep homeostasis and a dopamine arousal pathway in *Drosophila*. *PLoS Genet* **8**, e1003003.
- 15 Schwenk J, Metz M, Zolles G, Turecek R, Fritzius T, Bildl W, Tarusawa E, Kulik A, Unger A, Ivankova K *et al.* (2010) Native GABA(B) receptors are

- heteromultimers with a family of auxiliary subunits. *Nature* **465**, 231–235.
- 16 Bartoi T, Rigbolt KT, Du D, Kohr G, Blagoev B and Kornau HC (2010) GABAB receptor constituents revealed by tandem affinity purification from transgenic mice. *J Biol Chem* **285**, 20625–20633.
 - 17 Turecek R, Schwenk J, Fritzius T, Ivankova K, Zolles G, Adelfinger L, Jacquier V, Besseyrias V, Gassmann M, Schulte U *et al.* (2014) Auxiliary GABAB receptor subunits uncouple G protein betagamma subunits from effector channels to induce desensitization. *Neuron* **82**, 1032–1044.
 - 18 Adelfinger L, Turecek R, Ivankova K, Jensen AA, Moss SJ, Gassmann M and Bettler B (2014) GABAB receptor phosphorylation regulates KCTD12-induced K (+) current desensitization. *Biochem Pharmacol* **91**, 369–379.
 - 19 Dementieva IS, Tereshko V, McCrossan ZA, Solomaha E, Araki D, Xu C, Grigorieff N and Goldstein SA (2009) Pentameric assembly of potassium channel tetramerization domain-containing protein 5. *J Mol Biol* **387**, 175–191.
 - 20 Ji AX, Chu A, Nielsen TK, Benlekbir S, Rubinstein JL and Prive GG (2016) Structural insights into KCTD protein assembly and Cullin3 recognition. *J Mol Biol* **428**, 92–107.
 - 21 Smaldone G, Pirone L, Balasco N, Di Gaetano S, Pedone EM and Vitagliano L (2015) Cullin 3 recognition is not a universal property among KCTD proteins. *PLoS One* **10**, e0126808.
 - 22 Lange S, Perera S, Teh P and Chen J (2012) Obscurin and KCTD6 regulate cullin-dependent small ankyrin-1 (sAnk1.5) protein turnover. *Mol Biol Cell* **23**, 2490–2504.
 - 23 Balasco N, Pirone L, Smaldone G, Di Gaetano S, Esposito L, Pedone EM and Vitagliano L (2014) Molecular recognition of Cullin3 by KCTDs: insights from experimental and computational investigations. *Biochim Biophys Acta* **1844**, 1289–1298.
 - 24 Pirone L, Correale S, de Paola I, Zaccaro L, De Simone G, Vitagliano L, Pedone E and Di Gaetano S (2011) Design, synthesis and characterization of a peptide able to bind proteins of the KCTD family: implications for KCTD-cullin 3 recognition. *J Pept Sci* **17**, 373–376.
 - 25 Pirone L, Esposito C, Correale S, Graziano G, Di Gaetano S, Vitagliano L and Pedone E (2013) Thermal and chemical stability of two homologous POZ/BTB domains of KCTD proteins characterized by a different oligomeric organization. *Biomed Res Int* **2013**, 162674.
 - 26 de Paola I, Pirone L, Palmieri M, Balasco N, Esposito L, Russo L, Mazzà D, Di Marcotullio L, Di Gaetano S, Malgieri G *et al.* (2015) Cullin3-BTB interface: a novel target for stapled peptides. *PLoS One* **10**, e0121149.
 - 27 Tang G, Peng L, Baldwin PR, Mann DS, Jiang W, Rees I and Ludtke SJ (2007) EMAN2: an extensible image processing suite for electron microscopy. *J Struct Biol* **157**, 38–46.
 - 28 Brenner S and Horne RW (1959) A negative staining method for high resolution electron microscopy of viruses. *Biochim Biophys Acta* **34**, 103–110.
 - 29 Barone D, Balasco N and Vitagliano L (2015) KCTD5 is endowed with large, functionally relevant, interdomain motions. *J Biomol Struct Dyn* **19**, 1–11.

Supporting information

Additional Supporting Information may be found online in the supporting information tab for this article:

Appendix S1. Expression and purification of KCTD1, KCTD1^{BTB}, and KCTD13^{BTB}.

Fig. S1. FarUV CD spectra of KCTD1^{BTB} (black line) and full-length KCTD1 (red line).

Fig. S2. Secondary structure prediction of KCTD1^{BTB}.

Fig. S3. 2D reference-free class averages and rotational cross-correlation analysis of the KCTD5^{BTB} domain.

Fig. S4. Electron micrograph of a KCTD1^{BTB} sample negatively stained with uranyl acetate 2%.

Fig. S5. Electron micrograph of a KCTD6^{BTB} sample negatively stained with uranyl acetate 2%.

Fig. S6. Electron micrograph of a KCTD11^{BTB} sample negatively stained with uranyl acetate 2%.

Fig. S7. Electron micrograph of a KCTD12^{BTB} sample negatively stained with uranyl acetate 2%.

Fig. S8. Electron micrograph of a KCTD13^{BTB} sample negatively stained with uranyl acetate 2%.

Fig. S9. Electron micrograph of a KCTD15^{BTB} sample negatively stained with uranyl acetate 2%.